PCCP

Accepted Manuscript

ROYAL SOCIETY OF CHEMISTRY

www.rsc.org/pccp

Microsolvation of Methlymercury: Structures, Energies, Bonding and NMR Constants (^{199}Hg, ^{13}C and ^{17}O)

Edison Flórez,[†] Alejandro F. Maldonado,[‡] Gustavo A. Aucar,[*,‡] Jorge David,[¶] and Albeiro Restrepo[*,†]

Instituto de Química, Universidad de Antioquia UdeA, Calle 70 No. 52–21, Medellín, Colombia, Physics Department, Natural and Exact Science Faculty, Northeastern University of Argentina and Institute of Modelling and Innovation on Technology, IMIT, Corrientes, Argentina, and Departamento de Ciencias Físicas, Universidad EAFIT, Medellín, Colombia

E-mail: gaa@unne.edu.ar; albeiro.restrepo@udea.edu.co

[*]To whom correspondence should be addressed
[†]Universidad de Antioquia, Medellín, Colombia
[‡]Universidad Nacional del Nordeste, IMIT, Corrientes, Argentina
[¶]Universidad EAFIT, Medellín, Colombia

Abstract

Hartree–Fock (HF) and second order perturbation theory (MP2) calculations within the scalar and full relativistic frames were carried out in order to determine equilibrium geometries and interaction energies between cationic methylmercury (CH_3Hg^+) and up to three water molecules. A total of nine structures were obtained. Bonding properties were analyzed using the Quantum Theory of Atoms In Molecules (QTAIM). The analyses of the topology of the electron densities reveal that all structures exhibit a partially covalent Hg$\cdots$O interaction between methylmercury and one water molecule. Consideration of additional water molecules suggest that they solvate the $(CH_3Hg\cdots OH_2)^+$ unit. Nuclear magnetic shielding constants $\sigma(^{199}Hg)$, $\sigma(^{13}C)$ and $\sigma(^{17}O)$ were calculated, as well as indirect spin-spin coupling constant $J(^{199}Hg–^{13}C)$, $J(^{199}Hg–^{17}O)$ and $J(^{13}C–^{17}O)$, for each one of the geometries. Thermodynamic stability and the values of NMR constants correlate with the ability of the system to directly coordinate oxygen atoms from water molecules to the mercury atom in methylmercury and to the formation of hydrogen bonds among solvating water molecules. Relativistic effects account for 11% on $\sigma(^{13}C)$ and for 14% on $\sigma(^{17}O)$, these are due to the presence of Hg (heavy atom on light atom, HALA effect), while relativistic effects on $\sigma(^{199}Hg)$ are close to 50% (heavy atom on heavy atom itself, HAHA effect). J–coupling constants are highly influenced by relativity when mercury is involved as in $J(^{199}Hg–^{13}C)$ and $J(^{199}Hg–^{17}O)$. On the other hand, our results show that the values of NMR constants for carbon and oxygen, atoms which are connected through mercury (C–Hg$\cdots$O), are highly correlated and are greatly influenced by the presence of water molecules. Water molecules introduce additional electronic effects to the relativistic effects due to the mercury atom.

Introduction

Mercury exists in a wide variety of chemical forms, all of which are toxic. Even though the levels of toxicity vary, every form can affect the nervous, immune and reproductive systems [1, 2]. Once in contact with water, mercury transforms into methylmercury through the process of methylation, which mainly occurs in ocean and river sediments that are rich in organic materials [2–5]. It is difficult to overemphasize the importance of water in biological systems since water comprises 70–80% of the mass of all living organisms and since it is well known that water serves not only as medium in which all known biochemical processes occur, but also, in many cases, water is directly involved in such processes [6]. In their cationic forms, metals play important roles in biochemical processes because they are electron deficient species. Most biomolecules, such as proteins and DNA, contain readily available electrons, thus, biomolecule↔metallic cation interactions inside living organisms are highly favored. In the specific case of methylmercury, this chemical affinity is a source of great concern, to the point that several multinational treaties, such as the Minamata agreement [7, 8], aim at complete elimination of all mercury containing pollutants, to this end, mercury compounds have been banned from industrial and domestic applications.

Analyzing and describing CH_3Hg^+ behavior in aqueous environments, in other words, studying the microsolvation process of the methylmercury cation is necessary because of the need to understand the biochemical processes and macroscopic phenomena in which it is involved. Understanding the behavior of various forms of mercury, in particular methylmercury, is a first and important step for their appropriate handling and control. We offer in this work a detailed view of the structural, energetical, and bonding aspects involved in the microsolvation of methylmercury in aqueous environments, we supplement this information with very sophisticated calculations of the NMR constants, however, the phisiological and biological aspects of the interaction betwen mercury compounds and living organisms is a subject too broad and complex that falls outside the scope of this work.

Microsolvation with a finite number of water molecules may be considered as an intermediate between the gas phase and the condensed phase. Once enough solvent molecules are taken into account in microsolvation, the properties of the condensed state can be explained [9].

A convenient way of classifying molecular properties is to separate them into intrinsic and response properties. Intrinsic properties include excitation energies, thermodynamic properties, vibrational levels, molecular structures, etc. Response properties measure the effect of applied electromagnetic fields on a molecular system, these include polarizability, nuclear magnetic resonance parameters (nuclear magnetic shielding, σ and indirect spin-spin coupling, J), magnetic moments, etc. Regarding response properties, NMR spectroscopy is a common technique used to obtain detailed information about molecular structures due to the sensitivity of NMR parameters to chemical environments and to the high structure$\leftrightarrow$spectroscopy correlation. Magnetic properties in mercury compounds have been extensively studied by both experimental and theoretical methods. Nuclear magnetic shielding and indirect J-coupling constants have been determined in different mercury species for various purposes: structural determination [10–12], analysis of inter and intramolecular interactions [13–15] and the description of several electronic effects [16, 17]. NMR parameters have also been used to study the interactions between methylmercury and a number of biomolecules in order to understand the biological role of these substances [18–21].

To determine reliability of the results in computational studies of chemical systems, specifically in the study of microsolvation of methylmercury, three important approximations or aspects must be taken in account: the level of theory, solvent effects, and relativistic effects [22]. For example, solvent effects on nuclear shielding and on J coupling constants in methylmercury halides, CH_3HgX (X = Cl, Br, I) have been reported [13, 14]; detailed comparison of the experimental and calculated results reveal high sensitivity to environmental effects, good agreements are achieved

as long as solvent effects are considered in the computations. Solvent effects were also studied on $Hg(CN)_2$ and MeHgCl by Zheng and Autschbach at the ZORA level under ab initio molecular dynamics using the droplet model [23], they found deviations no larger than 6% between calculated and experimental J(^{199}Hg–^{13}C) in DMSO solvated MeHgCl and that solute↔solvent interactions dramatically increase the Hg–C coupling constants. Wolff and coworkers [24] used the ZORA Hamiltonian to study NMR shieldings in MeHgX (X=Me, CN, Cl, Br, I) and in HgY_2 (Y=CN, Cl, Br, I), they report calculated to experimental deviations of the order of 3% for ^{199}Hg. An excellent review on the calculations of NMR parameters in transition metal complexes has been offered by Autschbach [25]. Spin–Spin coupling in heavy metal (including mercury) compounds using the ZORA Hamiltonian was reported by Moncho and Autschbach [26]. On the other hand, in 2011 Arcisauskaite *et. al.* [16] investigated the importance of relativistic effects on σ(Hg) in linear mercury compounds HgL_2 (L = CH_3 , Cl, Br and I) considering different methodologies: 4–component (DFT), ZORA, LRESC [27, 28] (semi-relativistic methodology), and a non–relativistic method (NR). LRESC calculations for $HgCl_2$ were the only ones to reproduce the experimental values. However, 4–component and ZORA calculations reproduced the experimental tendency underestimating the experimental measurements.

To the best of our knowledge, there is no information in the scientific literature concerning the structures of microsolvated methylmercury, nothing is known either about the nature of the methylmercury↔water molecular interactions responsible for cluster stability, nor about the σ and J NMR constants for methylmercury in aqueous media. In view of the preceding discussion, we think that this is a sensible lack of information, which this paper attempts to remedy.

Theoretical methods and computational details

Relativistic polarization propagator

Any static second order molecular property can be studied with the relativistic (REL) formalism of polarization propagators [29–31]; non–relativistic (NR) methods can be safely employed when only light atoms are involved. One of the advantages of this approach is the fact that NR values can be obtained directly from relativistic calculations making c, the speed of light, scale to infinity. The *fully* relativistic expressions of NMR spectroscopic parameters are written as

$$\mathbf{J}_{MN} = \frac{e^2\hbar^2}{h}\gamma_M\gamma_N \left\langle\left\langle \frac{\alpha\times\mathbf{r_M}}{r_M^3}; \frac{\alpha\times\mathbf{r_N}}{r_N^3} \right\rangle\right\rangle \tag{1}$$

and

$$\sigma_M = e^2 \left\langle\left\langle \frac{\alpha\times\mathbf{r_M}}{r_M^3}; \alpha\times\mathbf{r}_G \right\rangle\right\rangle \tag{2}$$

where $\mathbf{J}_{MN}$ is the indirect $\mathbf{J}$ coupling tensor between nuclei M and N, and σ_M refers to the nuclear magnetic shielding tensor of nucleus M. The expressions above are fully relativistic given that retardation effects are not to be included due to their comparative (with respect to the leading relativistic effects) small contributions [32, 33]. From these equations one observes that only one electronic mechanism is involved in each of both NMR spectroscopic parameters. There is also no distinction between dia and paramagnetic terms [31].

All terms in equations (1) and (2) can be calculated at different levels of approach depending on the fluctuation potential, *i.e.*, pure zeroth order (PZOA), consistent first order or random phase approximation (RPA), second order level (SOPPA), etc. The fluctuation potential represents the difference between the Coulomb and the self consistent field (SCF) potential. As has been explained in some detail elsewhere [30, 31], polarization propagators do not arise from a wavefunction–based formalism, rather, they arise from path integral treatment, thus the

perturbative expansions give different terms when compared to the usual ones. Within polarization propagators, introduction of electron correlation up to first order is obtained at the RPA level of approach. The actual expressions are in this case the same as those obtained by the coupled Hartree–Fock scheme [30]. At the moment, only the relativistic RPA level, RelPPA–RPA has been implemented in the DIRAC code [34].

Kinetic Balance Prescriptions

From the time independent one–electron Dirac equation in a static external potential V provided by the nuclei in the Born–Oppenheimer frame, the relationship between the large and the small components of the four–component spinor can be obtained

$$\Psi^S = \frac{1}{2mc}\left[1+\frac{E-V}{2mc^2}\right]^{-1}(\boldsymbol{\sigma}\cdot\mathbf{p})\Psi^L \tag{3}$$

In the $c\rightarrow\infty$ limit, the square bracket approaches unity, resulting in

$$c\Psi^S = \frac{(\boldsymbol{\sigma}\cdot\mathbf{p})}{2m}\Psi^L \tag{4}$$

This condition is called the *kinetic balance* prescription and ensures that the kinetic energy is properly represented in the non–relativistic limit. Gaussian basis sets are used to ease calculations due the straightforward evaluation of multicenter integrals

$$G^{\alpha}_{nkm_j} = N\ \mathbf{r}_A^{n-1}\ e^{-\alpha r_A^2}\ \chi_{km_j}(\theta,\phi) \tag{5}$$

where N is a normalization constant, A refers to the nuclear center and χ_{km_j} is the angular part of the hydrogenic solution of the Dirac equation. From equation (4), for each large component function with angular quantum number ℓ, we get two small component functions with $\ell+1$ and $\ell-1$ angular momentum numbers

$$\Psi^L \propto \psi^L = \{G_\ell^\alpha\} \quad \Rightarrow \quad \Psi^S \propto \psi^S = \begin{cases} \{G_{\ell-1}^\alpha + G_{\ell+1}^\alpha\}; & (RKB) \\ \{G_{\ell-1}^\alpha \,;\, G_{\ell+1}^\alpha\}; & (UKB) \end{cases} \tag{6}$$

and from this, two different prescriptions follow. In the *Restricted Kinetic Balance* (RKB) approach, the small component basis set comes from the direct application of equation (4). This gives a 1:1 ratio between the large and the small components. In the *Unrestricted Kinetic Balance* (UKB) prescription, each Gaussian function generated is independently used as a basis function and produces an approximate 2:1 ratio between the large and the small components. This increases the size of the small components and extends the positronic space. The size of the small components is a very important issue in the calculations of magnetic properties because the diamagnetic portion of these properties, including nuclear magnetic shieldings are related to negative energy states [35].

Generating cluster candidate structures

A key step in the study of atomic or molecular clusters is a proper description of the Potential Energy Surface (PES). Finding equilibrium or minimum energy structures is a tremendously challenging problem because the number of minima in a given PES increases exponentially with the number of geometrical variables. In this work, we use the ASCEC [36] (Annealing Simulado con Energía Cuántica) method in order to explore the potential energy surfaces (PES) of methylmercury interacting with up to 3 water molecules, $[CH_3Hg(H_2O)_n]^+ \, n = 1,2,3$. ASCEC uses a simulated annealing procedure [37–39] to generate cluster candidate structures which undergo further optimization by gradient following techniques to locate local minima. ASCEC has been successfully used to treat a wide variety of chemical problems [6, 40–58]. A detailed description about the workings of ASCEC, including a discussion of the use of a modified Metropolis acceptance test and the generation of Markov chains in the space of intermolecular interactions can be found elsewhere [40, 41].

In this work, random explorations of the $[CH_3Hg(H_2O)_n]^+ n = 1,2,3$ PESs were carried out using the B3LYP hybrid functional in conjunction with the Stuttgart potential SDDALL to generate candidate structures. As an initial approach to understanding relativistic and correlation effects, two types of optimizations with traditional gradient–following methods of the candidate structures afforded by ASCEC were carried out. We performed scalar relativistic (SR) optimizations by using the GAUSSIAN 09 software [59], the candidate structures were also subject of relativistic (REL) optimizations using DIRAC 13 [34].

Scalar relativistic calculations

To select the level of theory that produces reliable results at a realistic computational cost, one of the candidate structures afforded by ASCEC for the $[CH_3Hg(H_2O)_3]^+$ system was optimized using the uncorrelated HF Hamiltonian and correlated methods, namely the B3LYP functional, second order perturbation theory (MP2), configuration interaction with single and double excitations (CISD) and its quadratic approach (QCISD), and coupled clusters with single and double excitations (CCSD). We used Stuttgart (SDDALL) and Los Alamos (LanL2DZ) potentials for mercury and the 6–311++G(d,p) basis set for all other atoms. The above mentioned calculations led us to select MP2. Thus, at the scalar relativistic level, MP2 in conjunction with SDDALL and LanL2DZ for Hg and the 6–311++G(d,p) basis sets for all other atoms was used to locate and characterize all stable minima within each PES. HF optimizations were also carried out to gain insight into the effect of electron correlation. The set of these two potentials and the 6–311++G(d,p) basis will be referred to as ECP in what follows without loss of generality. Characterization of each equilibrium structure as a true minimum was achieved through the calculation of analytical vibrational frequencies and analysis of the eigenvalues of the Hessian matrix in nuclear coordinate space. Additional energies with larger basis sets were calculated on the structural motifs (true HF, MP2, minima): aug–cc–pVTZ basis for H, C and O and the Def2–TZVPPD basis for Hg [60]. It is expected that these types of basis provide appropriate

treatment for Hg···O and for hydrogen bond interactions, both of which play stabilizing roles in the title systems. In a similar way to ECP, from now, the whole Def2–TZVPPD and aug–cc–pVTZ basis will be simply referred as Def2. Binding energies (BE) were calculated by subtracting the energy of each molecular motif from the sum of the energies of isolated constituents, that is, n times the energy of the water molecule plus the energy of isolated methylmercury. In this way, large positive BE values correspond to large binding energies. Relative energies (ΔE) were obtained by calculating the energy difference between a particular molecular motif and the energy of the global minimum in the corresponding PES. All relative and binding energies reported here were corrected by zero–point vibrational energies (ZPEs) at the MP2/ECP level.

The most common hypothesis about chemical bonds and molecular interactions is that these only depend on the valence electrons with little or no intervention of inner electrons. In this sense, ECPs are built and used. In ECPs, valence electrons are described by linear combinations of atomic orbitals while inner electrons (e.g. 60 for Hg) are described by using a core potential. Since relativistic effects mainly arise from inner electrons in heavy atoms, these are included in the potential.

Relativistic calculations

Relativistic optimizations were carried out by using the Dirac-Hartree–Fock Hamiltonian (DHF) in conjunction with the aug–cc–pVDZ basis for carbon, hydrogen and oxygen atoms, and the dyall.v2z basis for mercury. Basis sets were completely uncontracted and the nuclei were modeled as Gaussian distributions. Symmetry constraints were not used in the calculations for any of the motifs.

Relativisitc MP2 (Rel–MP2) was developed for a selection of Kramer–restricted DHF closed and open shell reference wavefunctions and was succesfully applied to the ground state of the O_2

molecule [61]. This procedure was extended and applied to the ground state of CuF, AgF and AuF. Relativistic bond contractions for AuF at the SCF and MP2 levels suggested that DHF should be revised to go beyond the independent particle model and include correlation [62]. In 2005, the first implementation of analytical first–order one–electron molecular properties at the Dirac–Coulomb MP2 level of theory was described. The method was applied to the calculation of parity violation energies in H_2X_2 (X = O, S, Se, and Te), it was shown that electron correlation does not play an important role for this property in those particular systems [63].

Results and discussion

Cluster structures

At the SR level, we located 1, 2, and 6 structures on the PES for $n = 1,2,3$ respectively. Due to the extremely high computational cost of full DHF calculations, we selected the most stable structures for $n = 1,2$ and the 4 lowest energy isomers for the $n = 3$ case obtained from the SR case and further optimized them at the full DHF level. Small to negligible changes when comparing SR vs full DHF molecular geometries justify not pursuing full relativistic optimizations on all clusters for all molecularities.

We adopt a simplistic, energy driven notation to classify the located clusters: we address the structures as W_nS_m, with n indicating the number of water molecules and m establishing relative stability; as an illustration of this notation, W_3S_4 refers to the fourth most stable structure for the interaction between methylmercury and three water molecules. A very similar notation is used to describe the structures found with the REL methodology: the geometries found with DHF are noted r–W_nS_m. Figure 1 shows the geometrical motifs obtained at the SR MP2/ECP level, together with notation and relative energies. Table 1 exposes the most relevant geometrical parameters obtained at the MP2/ECP level while Table 2 summarizes the effects of relativity and electronic correlation in the structures, there are no relevant geometrical changes in the spatial

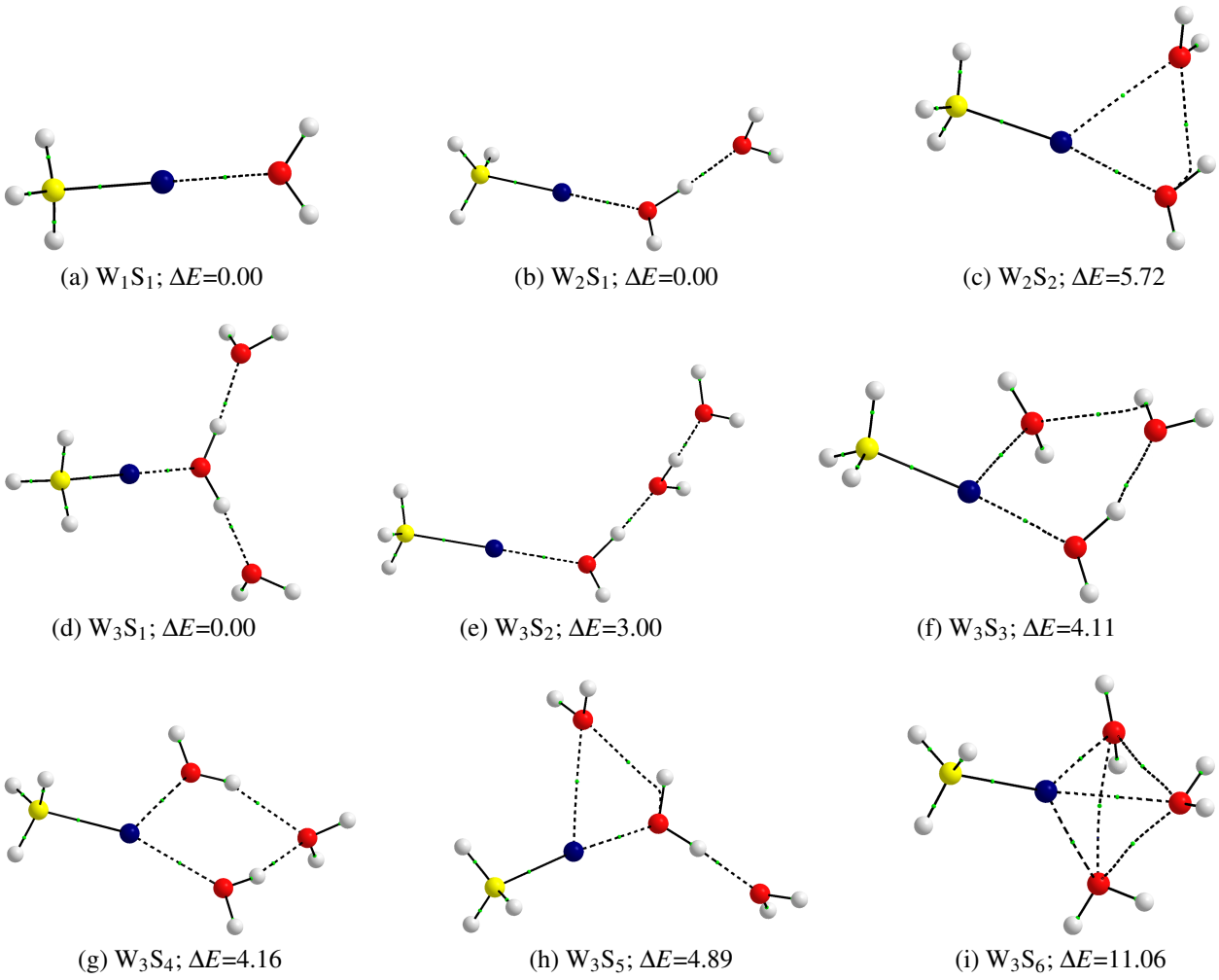

(a) W_1S_1; ΔE=0.00 (b) W_2S_1; ΔE=0.00 (c) W_2S_2; ΔE=5.72

(d) W_3S_1; ΔE=0.00 (e) W_3S_2; ΔE=3.00 (f) W_3S_3; ΔE=4.11

(g) W_3S_4; ΔE=4.16 (h) W_3S_5; ΔE=4.89 (i) W_3S_6; ΔE=11.06

Figure 1: Local minima in the PESs for the $[CH_3Hg(H_2O)_n]^+$ systems at the MP2/ECP SR level. ZPE corrected relative energies with respect to the global minimum within each PES are also included. Oxygen atoms in red, hydrogen atoms in white, carbon atoms in yellow and mercury atoms in blue. Bonding paths and intermolecular bond critical points (green dots) for all intermolecular interactions are also shown.

arrangements of the water molecules with regard to SR results.

At the MP2/ECP level, C–H bond lengths remain unchanged (1.09 Å) for all the motifs while Hg–C distances slightly change between 2.05 Å and 2.14 Å. We point out that regardless of the stoichiometry of the clusters, shorter Hg–C bond lengths are clearly seen in the low energy structures. The C–Hg–H angle remains almost constant around 23°, while the H–C–H angle marginally changes between 111° and 112°, characteristic of sp^3 hybridized carbons.

Table 1: Scalar relativistic MP2/ECP structural parameters for $[CH_3Hg(H_2O)_n]^+$ clusters. All bond lengths in Angstroms and all bond angles in degrees.

Parameter	W_1S_1	W_2S_1	W_2S_2	W_3S_1	W_3S_2	W_3S_3	W_3S_4	W_3S_5	W_3S_6
C–Hg	2.06	2.06	2.12	2.05	2.05	2.06	2.07	2.11	2.14
C–H	1.09	1.09	1.09	1.09	1.09	1.09	1.09	1.09	1.09
C–Hg–H	24	23	23	23	23	23	23	23	23
H–C–H	112	111	112	111	111	111	111	111	112

Table 2: Structural parameters determined within the relativistic frame for $[CH_3Hg(H_2O)_{1,2,3}]^+$. Bond lengths in Å bond angles in degrees. Experimental results by Kashiwabara and coworkers [64] refer to electron diffraction studies for the dimethylmercury gas phase case, while the work by Jokisaari and Diehl [12] involves NMR spectra of CH_3HgCl dissolved in liquid crystals.

	DHF					
Parameter	r-W_1S_1	r-W_2S_1	r-W_3S_1	r-W_3S_2	Experimental	
C–Hg	2.10	2.09	2.08	2.09	2.08[12]	2.08[64]
C–H	1.08	1.08	1.08	1.08	1.09[12]	1.11[64]
C–Hg–H	23	23	23	23	23[12]	
H–C–H	112	111	111	111	109[12]	109[64]

Excellent agreement between experimental non–solvated and calculated solvated geometries is obtained for CH_3Hg^+. Comparing our geometries with the ones experimentally determined via NMR [10–12] and electron diffraction [64], differences no larger than 4% are observed. This means that the CH_3Hg^+ geometry is not very sensitive to interactions with the solvent. It is seen that full relativistic DHF geometrical variables are quite similar to the ones obtained with SR MP2/ECP and that both reproduce the experimental results for non–solvated CH_3Hg^+ with slight differences. At the REL level, C–H bond lengths remain unchanged (1.08Å), while C–Hg bonds remain close to 2.10Å; C–Hg–H angles change between 22° and 23° and the H–C–H angles remain $\approx 112°$.

O–H bonds not taking part in hydrogen bonding do not change their lengths to any appreciable degree, remaining close to 1.0 Å. On the other hand, hydrogen bond distances ($H_2O\cdots$H–O–H) cover the 1.48–2.32 Å range. The 0.84 Å window for hydrogen bond distances in the $[CH_3Hg(H_2O)_{1,2,3}]^+$ complexes allows a wide spectrum of geometric possibilities and interaction energies.

Two types of Hg$\cdots$O contacts are discerned from Figure 1: on one hand, there are those for which the C–Hg$\cdots$O angle is close to 180°, these are seen in all structures, on the other hand, there are those for which the C–Hg$\cdots$O angle is substantially smaller than 180°, usually close to 120°, these appear in all cases where a second water molecule is in direct contact with Hg (see structures W_2S_2, W_3S_3, W_3S_4, W_3S_5, W_3S_6 in Figure 1). These two types of Hg$\cdots$O interactions are not only geometrically distinguishable, they also have very different origins and nature as will be discussed later.

Table 1 and Table 2 suggest that in view of the demanding computational cost of full relativistic geometry optimizations, SR geometries are acceptable, with minor to negligible changes among the two sets of geometries. Interaction energies (Table 3) on the other hand seem to be more sensitive to relativistic effects and to the proper description of electron correlation. SR HF underestimates BEs by up to 14 kcal/mol when compared to SR MP2 calculations, however, in the relativistic case, DHF BEs exceed Rel$-$MP2 BEs by up to 17 kcal/mol. Furthermore, our results suggest that relativistic effects and electron correlation need both be included for accurate calculations of interaction energies which are overestimated by up to 17 kcal/mol in DHF//HF when compared to Rel$-$MP2//MP2 (Table 3). Table 3 lists BEs at the SR and full relativistic (DHF) levels. When electron correlation at the MP2 level is included in the SR calculations, BEs increase by $\approx$ 20% for all molecules, this is in very good agreement with what has been found in other molecular systems [65, 66]. On the other hand full relativistic BEs are slightly larger ($\approx$ 1

kcal/mol) than those calculated at the SR level, this is also in agreement with previous resuls reported for molecules containing heavy atoms [67]. However, opposite results are obtained when MP2 electron correlation is conisdered in the full relativistic calculations, leading to severe overestimation of binding energies in the SR regime.

Table 1 and Table 2 show very small differences in geometries at the SR and DHF levels, specially in those bonds wehre Hg is involved, thus the largest enlargement of the Hg–C bond is around 0.04 Å. Since the effect of relativity in the calculated molecular geometries is so small, we argue that differences in binding energies could be attributed to electron correlation. In any case, our calculations show that there is an interplay between electron correlation and relativistic effects so that they cannot be considered as independent. This dependecy among both effects has been documented for molecular properties in molecules containing heavy atoms [68, 69]. This behaviour was also found in calculations on the XeF_2 molecule, where relativistic and electron correlation effects acting together produce a decrease of ≈ 2 eV in BE and an enlargement of the Xe–F bond distance, which is in conflict with the knwon general trends for both effects [70]. On the other hand, in our particular case, both SR–MP2 and Rel–MP2 calculations suggest that relativistic effects at the SR level contribute in oposite way to the spin orbit (SO)coupling. Furthermore, SR–MP2 values follow the same trend as non–relativistic values including electron correlation.

Table 3: Energetic analysis ($kcal/mol$) for the $[CH_3Hg(H_2O)_{1,2,3}]^+$ systems. m is the number of Hg$\cdots$O contacts. h is the number of the hydrogen bonds. BE: binding energy. All MP2/Def2 energies corrected for the MP2/ECP unscaled ZPEs. Relativistic single point energies were calculated at the Rel−MP2 level on the MP2/ECP optimized geometries and DHF energies were calculated on the HF/ECP geometries. The aug–cc–pVDZ (H, C, O) and dyall.v2z (Hg) basis set were used.

			Scalar Relativistic				**Relativistic**			
			Optimization				Energies		Optimization	Energies
			HF		MP2		DHF//HF	Rel–MP2//MP2	DHF	Rel–MP2//DHF
Structure	m	h	BE	BE+ZPE	BE	BE+ZPE	BE	BE	BE	BE
W_1S_1	1	0	29.29	27.14	34.96	32.92	32.60	23.73	30.03	20.68
W_2S_1	1	1	45.15	40.51	55.28	50.61	48.04	33.53	46.00	30.99
W_2S_2	2	0	42.39	37.92	49.55	44.99	45.79	31.19		
W_3S_1	1	2	58.81	52.01	72.61	65.61	61.51	44.17	59.80	42.20
W_3S_2	1	2	55.56	48.80	69.61	62.62	57.84	40.82	56.50	39.16
W_3S_3	2	2			68.49	61.44		40.01	57.24	39.68
W_3S_4	2	2	55.64	48.76	68.44	61.49	58.98	41.66	57.17	39.44
W_3S_5	2	1	56.74	49.98	67.72	60.39	59.51	42.28		
W_3S_6	3	0	51.64	45.17	61.55	54.53	54.86	37.48		

Topological analysis of electron densities

As discussed above, thermodynamic stability of $[CH_3Hg(H_2O)_n]^+$ clusters is primarily determined by the nature of water↔methylmercury interactions and by hydrogen bonds among water molecules. These types of intermolecular interactions keep the complexes as discrete molecular entities. The interactions considered in this work are not assigned upon visual inspection of the structures in Figure 1, rather, they correspond to well defined bonding paths for intermolecular interactions as determined by the Quantum Theory of Atoms in Molecules (QTAIM) [71]. All topological properties of the electron densities were calculated using the AIMStudio suite [72] on the MP2/ECP optimized geometries (Figure 1).

QTAIM provides a universal definition for what constitutes bonding. QTAIM formalism characterizes interactions as a result of closed–shell (ionic, hydrogen bond, etc.), shared (covalent), and intermediate interactions (with contributions from both closed shell and shared interactions). To describe bonding interactions, information at bond critical points (BCPs) was gathered, this includes electron densities $\rho(\mathbf{r}_c)$, their corresponding Laplacians $\nabla^2\rho(\mathbf{r}_c)$, as well as potential $\mathscr{V}(\mathbf{r}_c)$, kinetic $\mathscr{G}(\mathbf{r}_c)$ and total energy densities $\mathscr{H}(\mathbf{r}_c)$. There are exotic O$\cdots$O interactions in W_2S_2, W_3S_5 and W_3S_6, these interactions are known to occur in other systems [73, 74], specifically in water clusters [75] and are known to be comparatively weaker than hydrogen bonds and thus will not be analyzed in this work. Very recently, similar long range S$\cdots$S interactions have been discovered in H_2S clusters [58]. Quantification of the relative strength of the Hg–C, Hg$\cdots$O, H–O and H2O$\cdots$H–O–H interactions was achieved using the criteria explained next.

The Laplacian of the electron density

$\nabla^2\rho(\mathbf{r}_c)$, the Laplacian of the electron density at bond critical points is related to the interaction energy by a local expression of the virial theorem by

$$\left(\frac{\hbar^2}{4m}\right)\nabla^2\rho(\mathbf{r}_c) = 2\mathscr{G}(\mathbf{r}_c) + \mathscr{V}(\mathbf{r}_c) \tag{7}$$

Where $\mathscr{G}(\mathbf{r}_c)$ is always positive and $\mathscr{V}(\mathbf{r}_c)$ is always negative. $\nabla^2\rho(\mathbf{r}_c)$ at a BCP is determined by the 2:1 virial ratio between both forms of energy. BCPs are local extrema of the electron density, thus, the sign of the Laplacian affords valuable information about the nature of the interaction: positive Laplacians correspond to local minima, which means that there is charge depletion at the BCP and charge concentration towards the nuclei, this is typical of long range and ionic interactions; on the other hand, negative Laplacians correspond to local maxima in the electron density, meaning that there is charge concentration in the intermediate region between the involved nuclei, around the BCPs, which is characteristic of shared or covalent interactions [71, 76]. Even though the virial theorem can be derived from an effective relativistic Hamiltonian, we consider here that the electron density at a bond critial point is closely related to the behavior of valence electrons. It is known that valence electrons resemble the NR behavior, thus, Eq. 7 is still valid within the relativistic regime.

Table 4 and Table 5 show the Laplacians computed at all BCPs. For the complexes formed by water $\leftrightarrow$ CH_3Hg^+ interactions, H–O interactions within water molecules are the only ones exhibiting negative Laplacians at the BCPs (not shown in Tables), all other interactions (Hg–C, H2O$\cdots$H–O–H and Hg$\cdots$O) have positive Laplacians, thus, according to this criterion, all interactions should be classified as long range or ionic.

Total energy density

The total electronic energy density at a BCP can be used to estimate the strength of the interaction [77]. $\mathscr{H}(\mathbf{r}_c)$ is negative for all interactions with shared electrons and its magnitude measures the covalent character. On the other hand, $\mathscr{H}(\mathbf{r}_c)$ is positive for the cases in which $\mathscr{G}(\mathbf{r}_c)$, the kinetic energy density, is larger than $\mathscr{V}(\mathbf{r}_c)$, the potential energy density, a condition that is characteristic

Table 4: Topology of the electron densities for the $[CH_3Hg(H_2O)_{1,2,3}]^+$ complexes. All values obtained at BCPs for the corresponding interactions.

Structure	Length [Å]	$\rho(r_c)$ $[10^{-1}]$ au	$\nabla^2\rho(r_c)$ $[10^{-1}$ au]	$\mathscr{H}(r_c)$ $[10^{-2}$ au]	$\lvert\mathscr{V}(\mathbf{r}_c)\rvert/\mathscr{G}(\mathbf{r}_c)$	δ(Hg–X)
Hg–C BCPs						
W_1S_1	2.06	1.29	0.35	−6.42	1.88	1.05
W_2S_1	2.06	1.32	0.42	−6.66	1.87	1.05
W_2S_2	2.12	1.14	1.00	−5.37	1.95	1.02
W_3S_1	2.05	1.34	0.50	−6.78	1.85	1.05
W_3S_2	2.05	1.33	0.47	−6.73	1.86	1.05
W_3S_3	2.06	1.32	0.57	−6.55	1.83	1.04
W_3S_4	2.07	1.29	0.64	−6.29	1.80	1.05
W_3S_5	2.11	1.12	1.05	−5.58	1.95	1.02
W_3S_6	2.14	1.11	1.18	−4.93	1.86	1.01
Hg···O [§] BCPs						
	C–Hg···O angle $\approx 180°$					
W_1S_1	2.23	0.62	3.48	−0.23	1.03	0.37
W_2S_1	2.17	0.73	4.07	−0.55	1.05	0.44
W_2S_2	2.27	0.60	3.40	−0.44	1.06	0.34
W_3S_1	2.14	0.81	4.47	−0.85	1.07	0.49
W_3S_2	2.15	0.78	4.28	−0.71	1.06	0.47
W_3S_3	2.18	0.73	3.99	−0.25	1.02	0.43
W_3S_4	2.23	0.64	3.53	−0.28	1.03	0.37
W_3S_5	2.21	0.71	4.02	−0.75	1.09	0.40
	C–Hg···O angle $< 180°$					
W_2S_2	2.72	0.23	1.00	0.04	0.98	0.14
W_3S_3	2.86	0.17	0.71	0.15	0.90	0.12
W_3S_4	2.59	0.29	0.14	0.22	0.93	0.18
W_3S_5	2.78	0.20	0.88	0.06	0.97	0.13
	Three equivalent Hg···O BCPs					
W_3S_6	2.51	0.36	1.80	-0.06	1.02	0.21

[§] W_2S_2,W_3S_3, W_3S_4, and W_3S_5 have two different Hg···O BCPs one of them with a C–Hg···O $\approx 180°$. W_3S_6 has three equivalent Hg··· BCPs. Figure 1.

Table 5: Topology of the electron densities for the $[CH_3Hg(H_2O)_{1,2,3}]^+$ complexes. All values obtained at BCPs for $H_2O\cdots HOH$ hydrogen bonds. As a reference, we calculated $|\mathscr{V}(\mathbf{r}_c)|/\mathscr{G}(\mathbf{r}_c)$ and $\delta(H_2O\cdots HOH)$ for the water dimer to be 1.03 and 0.06 respectively.

Structure	Length	$\rho(\mathbf{r}_c)$	$\nabla^2\rho(\mathbf{r}_c)$	$\mathscr{H}(\mathbf{r}_c)$	$\lvert\mathscr{V}(\mathbf{r}_c)\rvert/\mathscr{G}(\mathbf{r}_c)$	$\delta(H_2O\cdots HOH)$
BCP $H_2O\cdots HOH$						
W_2S_1	1.59	0.52	1.78	-0.69	1.14	0.10
W_3S_1	1.65	0.44	1.65	-0.26	1.06	0.09
	1.65	0.44	1.65	-0.26	1.06	0.09
W_3S_2	1.48	0.71	1.91	-1.87	1.28	0.12
	1.72	0.36	1.48	0.05	0.99	0.08
W_3S_3	1.59	0.53	1.78	-0.69	1.14	0.10
	2.32	0.12	0.47	0.21	0.79	0.02
W_3S_4	1.75	0.35	1.39	0.07	0.98	0.08
	2.06	0.18	0.78	0.28	0.83	0.04
W_3S_5	1.64	0.44	1.64	0.20	0.95	0.09

of closed shell interactions (equation 8).

$$\mathscr{H}(\mathbf{r}_c) = \mathscr{V}(\mathbf{r}_c) + \mathscr{G}(\mathbf{r}_c) \tag{8}$$

The results in Table 4 show the two types of water↔ methylmercury interactions mentioned above.

Those for which the C–Hg$\cdots$O angle is close to 180° (common to all clusters) all have negative energy densities at the Hg$\cdots$O BCPs, suggesting a high degree of electron sharing. Interactions for which the C–Hg$\cdots$O angle is smaller than 180°, all have positive energy densities at the Hg$\cdots$O BCPs, indicative of long range interactions with little electron sharing. These results suggest that only one water molecule is needed to stabilize CH_3Hg^+, put in other words, the interaction of CH_3Hg^+ with just one water molecule produces a bond in an advanced state of formation, further addition of water molecules then solvate the $(CH_3Hg\cdots OH_2)^+$ complex via hydrogen bonding between water molecules or via weaker Hg$\cdots$O contacts. This observation

nicely helps explaining the preferred coordination number of 2 for Hg in the title clusters; additional support for this claim will be given next in the discussions of other QTAIM descriptors.

It has been very well documentd that it is not uncommon for the signs of $\nabla^2\rho(\mathbf{r}_c)$ and of $\mathscr{H}(\mathbf{r}_c)$ give conflicting information, as a result, alternative schemes that combine both criteria have been suggested [78]. For example, Cremer and Kraka [77] pointed out that in some cases where the Laplacians of the electron density at BCPs are positive (local depletion of charge), the interaction can still be considered as covalent if the total energy density at the BCP is negative because the absolute value of the potential energy density exceeds the kinetic energy density, resulting in an overall stabilization of the BCP. Rozas and coworkers [79] suggested a more general set of criteria to determine the nature of interactions for hdrogen bonding cases, which are applicable to this work, they argue that weak to medium strength hydrogen bonds are characaterized by $\nabla^2\rho(\mathbf{r}_c) > 0$ and $\mathscr{H}(\mathbf{r}_c) > 0$ simultaneously, strong HBs exhibit $\nabla^2\rho(\mathbf{r}_c) > 0$ and $\mathscr{H}(\mathbf{r}_c) < 0$ and the very strong HBs have $\nabla^2\rho(\mathbf{r}_c) < 0$ and $\mathscr{H}(\mathbf{r}_c) < 0$. These all afford qualitative descriptions of the relative strengths of chemical interactions, in addition, in this work, we use the delocalization index [80] and the quantitative scale suggested by Espinosa and coworkers [81], both discussed next.

Delocalization index

The Delocalization index is another property that can be used to characterize bonding interactions [80]. The delocalization index, δ(A–B), measures the number of shared (delocalized) electrons between atoms A and B. In this work we use δ(Hg–X), X = C, O. There is a correlation between δ(A–B) and bond order: if δ(A–B) ≈ 1, a single bond is predicted, for δ(A–B) ≈ 2 a double bond is expected, and so on. Our calculations (Table 4, Table 5) afford δ(Hg–C) ≈ 1, suggesting a single bond between carbon and mercury in every complex. In addition, δ(Hg$\cdots$O) is between 0.34 and 0.49 in all cases where the C–Hg$\cdots$O angle is close to 180°, which is consistent with the picture of partially covalent interactions exposed above. For Hg$\cdots$O interactions having C–Hg$\cdots$O angles

$< 180^\circ$, $\delta(\mathrm{Hg}\cdots\mathrm{O}) \leq 0.2$, indicating weaker long range interactions.

The $|\mathscr{V}(\mathbf{r}_c)|/\mathscr{G}(\mathbf{r}_c)$ ratio

In 2002, Espinosa and coworkers proposed a method to discriminate the nature of interactions by local application of the virial theorem [81]. Their criterion suggests that $|\mathscr{V}(\mathbf{r}_c)|/\mathscr{G}(\mathbf{r}_c)$, the ratio of potential to kinetic energy densities evaluated at bond critical, can be divided into three regions affording information about the nature of bonding: the [0, 1] interval defines closed shell interactions (very little electron sharing), values larger than two correspond to increasingly covalent interactions, and the [1,2] interval encloses interactions wit contributions from both closed shell and shared interactions. It has been pointed out that neither the virial nor the kinetic energy are uniquely defined for arbitrary regions of space [71], therefore, the information they carry at critical points should not be overstated, nonetheless, Espinosa's criteria have successfully been applied to a variety of bonding situations. In this work, the $|\mathscr{V}(\mathbf{r}_c)|/\mathscr{G}(\mathbf{r}_c)$ ratio is an additional piece of evidence to support our view of the nature of intermolecular interactions. As seen in Table 4 and in Table 5, all Hg$\cdots$O interactions for which the C–Hg$\cdots$O angle is close to 180° have ratios that place them in the intermediate character, while those for which the C–Hg$\cdots$O angle is smaller than 180° fall into the closed shell (long range) nature. Very interesting is the effect of the formal charge in hydrogen bonds of the solvating water molecules, according to this criterion, some of them are unusually strong, being characterized as of intermediate character. The effect of the formal charge in the entire system in discussed next.

The effect of the formal charge

Regardless of the number of water molecules, the most stable motifs in each stoichiometry are those having a single Hg$\cdots$O interaction, that is, the preferred coordination number of methylmercury is 1. This is very unusual and interesting because the formal positive charge acts as a strong attractor for lone pairs in water molecules, thus, multiple solvent attacks on the same solute molecule should be expected. This is the case for example for the microsolvation of metal

cations from groups I and II in the Periodic Table [46, 50], where up to 6 water molecules are needed to stabilize the formal positive charges. Similar coordination numbers larger than 1 are reported for the microsolvation of anions, even in molecules of considerable size like dimethylphosphate [49, 82] and Ibuprofen [55]. For mercury containing molecules, the coordination number is also usually larger than 1 [83–91], however, the mechanism of microsolvation of these neutral species is very different than for methylmercury because of the pressence of the formal charge. In the case of CH_3Hg^+, the stabilization mechanism is the same as in the microsolvation of other cations, namely, an ion↔dipole interaction is at play, the formal charge (ion) is stabilized via interaction with the dipole components of surrounding water molecules, specifically at the lone pair ends.

The seemingly odd and unusual preferred coordination number for methylmercury is rationalized with the help of the data in Table 4 as follows: the calculated delocalization indices for Hg$\cdots$O interactions are 0.37, 0.44, 0.49 for W_1S_1, W_2S_1, W_3S_1, the lowest energy structures for $n = 1,2,3$ respectively. These delocalization indices suggest that the Hg$\cdots$O interactions in the lowest energy structures are very strong (almost half a bond has been formed!), the strength of the interactions is also supported by high values of electron densities, their Laplacians, total energy densities at the BCPs, the $|\mathscr{V}(\mathbf{r}_c)|/\mathscr{G}(\mathbf{r}_c)$ ratios, and by the fact that Hg$\cdots$O distances are no larger than 8.5% than formal Hg–C bonds in the same clusters. Thus, we argue that a strong Hg$\cdots$O bond is highly formed between methylmercury and the first water molecule, and that other water molecules then microsolvate the $(CH_3Hg\cdots OH_2)^+$ complex.

The unusually short and long hydrogen bond distances are also a consequence of the formal positive charge in the solute. The very short distances (Figure 1, Table 5), all correspond to interactions between a water molecule in a second solvation shell and the water molecule directly in contact with methylmercury: since the Hg$\cdots$O interaction has already been described as very strong, it weakens the O–H bond making the proton more acid and more susceptible to attack by a

lone pair from a second water molecule, resulting in an unusually strong and short hydrogen bond (HB). Longer and weaker HBs (for example structures W_3S_3, W_3S_4 in Figure 1, Table 5) are the result of what could be considered a second solvation shell water molecule donating a proton for a HB with a third solvation shell water molecule, whose ability to form HBs has already been diminished by a weaker Hg$\cdots$O interaction.

NMR spectroscopic parameters

When the molecular systems under study contain atoms belonging to the fifth row of the Periodic Table or below, it is essential to include relativistic effects to obtain reliable results in the calculations of NMR parameters. We first analyse the non–relativistic limit of the nuclear magnetic shieldings, $\sigma(^{13}C)$, $\sigma(^{17}O)$ and $\sigma(^{199}Hg)$, and the behavior of the J-coupling constants $J(^{13}C–^{17}O)$, $J(^{199}Hg–^{13}C)$ and $J(^{199}Hg–^{17}O)$ belonging to W_1S_1 when the speed of light is scaled by a factor of λ (λc; $c = 137.0359998$ au), with increased values of λ. In what follows,^{17}O refers only and exclusively to the oxygen atom forming a C–Hg$\cdots$O angle close to 180°, unless otherwise specified.

Relativistic effects on the nuclear magnetic shielding σ and J-coupling constants of different atoms involved may be due to two phenomena: the so called HALA [92, 93] (*heavy atom effect on a light atom*), which modifies the light atom environment when there are heavy atoms in its vicinity, and the HAHA [94, 95] (*heavy atom effects on heavy atom itself*) which acts over the heavy atom itself. There is a third effect proposed recently called HAVHA [96] (*heavy atom effect on vicinal heavy atom*) that appears in molecular systems containing more than one heavy atom, but in this work, mercury is the only heavy atom. We have shown in previous works [69, 97] that polarization propagators at the RPA level of approach give reliable results when compared with experiments. This happens to heavy–atom containing molecular systems with Sn and Pb. This approach has proven superior to describe the pattern of chemical shifts when compared to DFT methods.

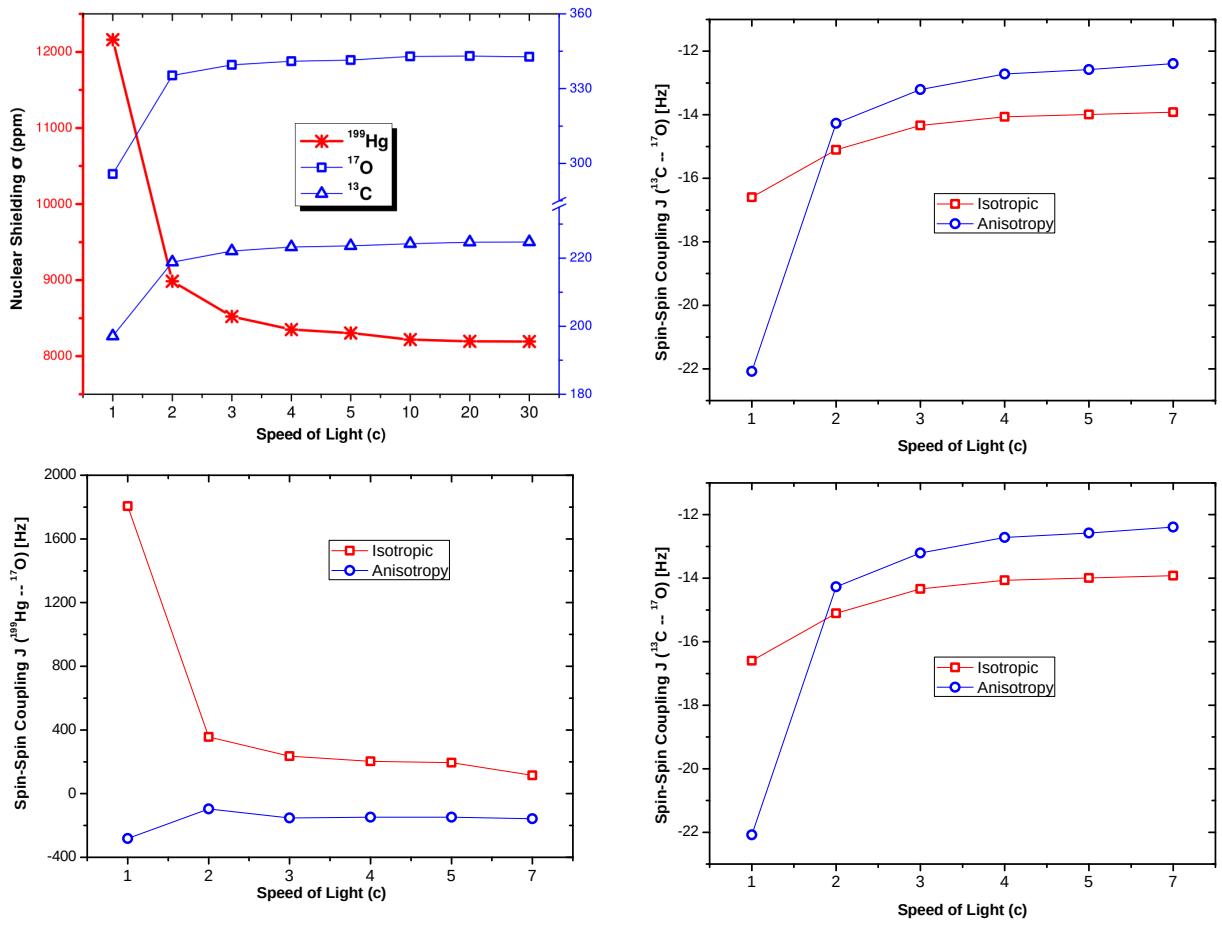

Figure 2: Relativistic values for nuclear shielding (σ, top left) and J-couplings as a function of the speed of light in W_1S_1. σ calculations using UKB and cc–pVTZ basis for C, O and dyall.v3z basis for Hg. J-coupling calculations using optimized aug–cc–pVTZ–J basis for C, O and H and dyall.v3z basis for Hg.

The results in Figure 2 and in Table 6 show that $\sigma(^{199}\text{Hg})$ rapidly decreases and converges to the non–relativistic limit value as λ increases. In addition, relativistic effects are positive and account for up to 48.6% of the total shielding (HAHA effect). On the other hand $\sigma(^{13}\text{C})$ and $\sigma(^{17}\text{O})$ exhibit an opposite to $\sigma(^{199}\text{Hg})$ dependency on relativistic effects (HALA effect). Those are negative but decrease the nuclear shielding of C and O by 10.7%, 13.6% respectively. Usually the HALA effects increase the magnitude of magnetic shielding on the ligh atom, but in this case the tendency is opposite.

Table 6: Relativistic (REL) and non–relativistic (NR) values of the nuclear magnetic shielding σ for ^{13}C, ^{17}O, and ^{199}Hg nuclei and the indirect J-coupling J(^{13}C$-^{17}$O), J(^{199}Hg$-^{17}$O) and J(^{199}Hg$-^{13}$C) in W_1S_1.

	σ (ppm)			**J** (Hz)			
				REL		NR	
Nucleus	REL	NR	**Nuclei**	Iso	Aniso	Iso	Aniso
^{13}C	197.11	220.74	^{13}C$-^{17}$O	-16.60	-22.08	-11.11	-11.29
^{17}O	295.72	342.31	^{199}Hg$-^{13}$C	3594.78	2923.11	2061.97	1221.63
^{199}Hg	12162.05	8182.50	^{199}Hg$-^{13}$O	1805.56	-281.49	237.29	-139.37

§ Iso and Aniso are short for the Isotropic and Anisotropic components of J-coupling respectively.

Figure 2 also shows the variation of J(^{13}C$-^{17}$O), J(^{199}Hg$-^{17}$O), and J(^{199}Hg$-^{13}$C) when the speed of light is scaled up to $7c$. As in the case of σ, the values rapidly converge to the NR limit. ^{2}J(^{13}C$-^{17}$O) is negative, as expected, while ^{1}J(^{199}Hg$-^{17}$O) and ^{1}J(^{199}Hg$-^{13}$C) are positive. Table 6 shows that relativistic effects on $^2J_{Iso}$(^{13}C$-^{17}$O) amount to $\approx$ 50% and to $\approx$ 74% on $^1J_{Iso}$(^{199}Hg$-^{13}$C), while for $^1J_{Iso}$(^{199}Hg$-^{13}$O) the relativistic value are more than seven times the non-relativistic one. As would be expected, relativistic effects in σ and J-coupling are of fundamental importance for accurate calculation of NMR parameters for the Hg atom, while for C and O, they are not negligible.

For the nine geometrical motifs shown in Figure 1, we conclude, from an electronic point of view, that the existence of partially covalent Hg$\cdots$O interactions and of hydrogen $H_2O\cdots$H–O–H hydrogen bonds, provide stability to the clusters and allow the complexes to behave as discrete units. From a structural point of view, we concluded that the interactions between CH_3Hg^+ and water molecules do not significantly change the geometric parameters (bond lengths and angles) of methylmercury (see Table 1 and Table 2). Thus, the spatial arrangement of the H_2O molecules and the Hg$\cdots$O interaction did not end up being crucial to modify the structure of CH_3Hg^+. However, Figure 3 shows that the interactions between water molecules and the water$\leftrightarrow$

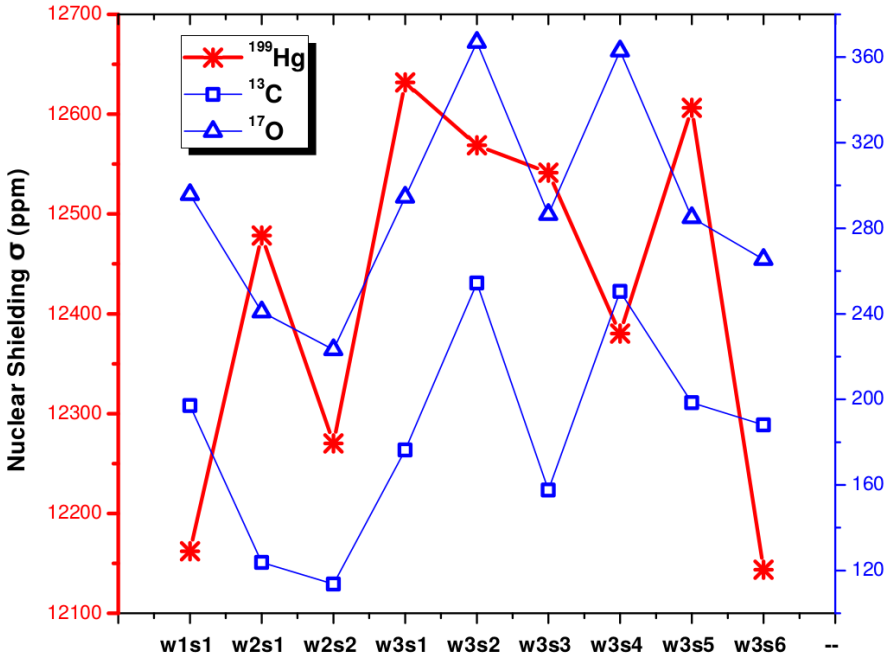

Figure 3: Nuclear shielding for ^{199}Hg, ^{13}C, ^{17}O, in all clusters reported in this work.

methylmercury interactions, together with the spatial arrangement of water molecules greatly influence the nuclear shielding on carbon and oxygen. The solvent introduces additional electronic effects to the effects of heavy atoms due to Hg.

There is a strong correlation between $\sigma(^{13}C)$ and $\sigma(^{17}O)$, hence, solvent effects, spatial arrangements as well as different types of interactions between water molecules, influence in a similar way the ^{17}O and ^{13}C atoms. These atoms are separated by two bonds. Nonetheless, the solvent induces electronic effects along the C–Hg$\cdots$O interaction, suggesting that the Hg atom serves as an electronic link between the C and O atoms. On the other hand, $\sigma(^{199}Hg)$ decreases as the coordination number in mercury increases. In addition, Figure 3 also shows a direct correlation between the shielding and the energy of each complex within a particular PES with the possible exception of W_3S_5. There is not a direct correlation between $\sigma(^{199}Hg)$ and the number and spatial disposition of hydrogen bonds, but the absence of hydrogen bonds is related with small values of $\sigma(^{199}Hg)$ and vice versa.

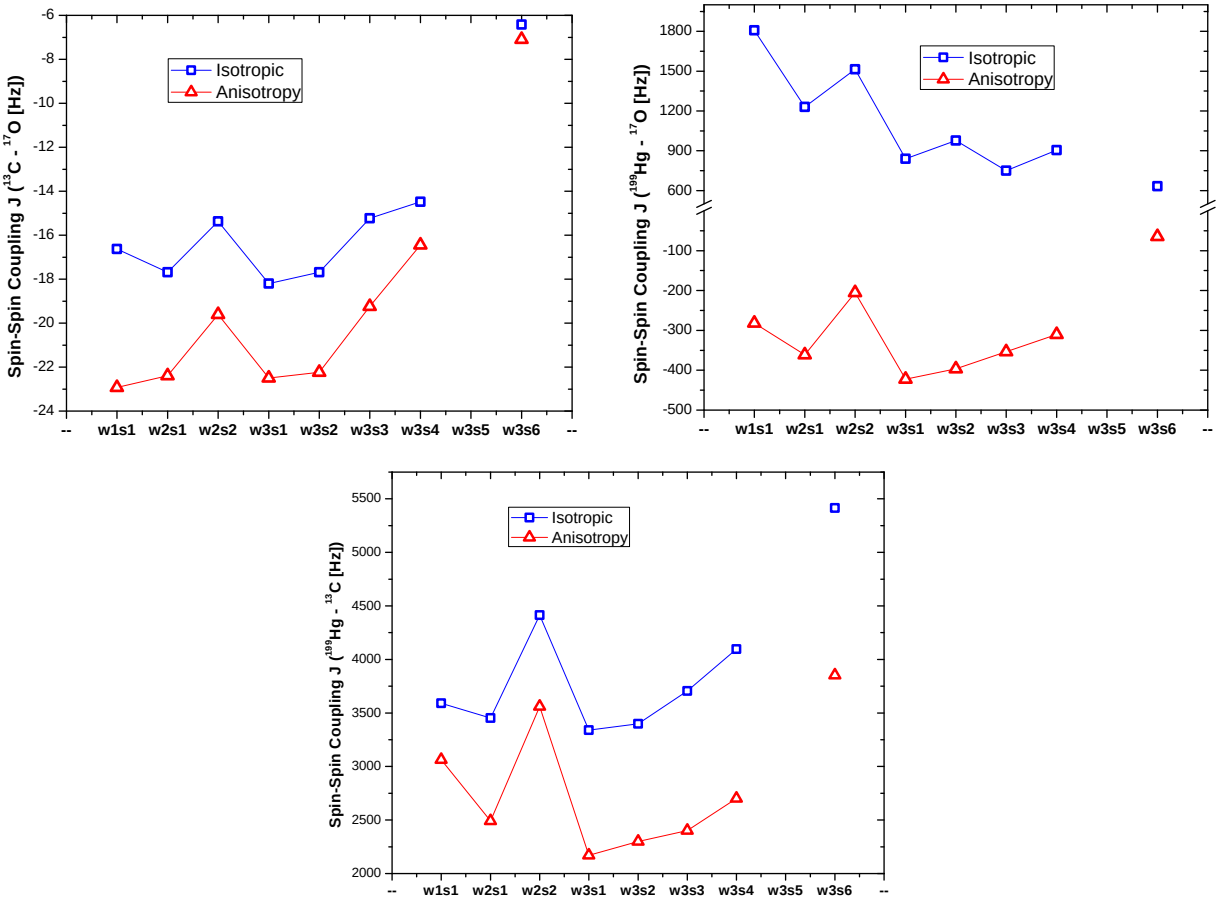

Figure 4: Relativistic calculations of J(^{13}C−^{17}O) (left), J(^{199}Hg−^{17}O) (middle) and J(^{199}Hg−^{13}C) (right) for the nine minima located in this work for the $[CH_3Hg(H_2O)_{1,2,3}]^+$ systems. Only the C–Hg···O interactions with an angle close to 180° are considered. Geometries taken from the MP2/ECP SR calculations. Relativistic calculations (DHF) using the dyall.v3z basis set for mercury and the aug–cc–pVTZ–Jun1 [98] basis set for C, O and H.

Figure 4 summarizes the calculated J-coupling constants for all clusters in this work. It is seen that the solvent affects J(^{13}C−^{17}O), J(^{199}Hg−^{17}O), and J(^{199}Hg−^{13}C). W_2S_2 and W_3S_6 comprise extreme cases: it is seen that J(^{13}C−^{17}O) and J(^{199}Hg−^{13}C) are maxima (both isotropic and anisotropic) for these two motifs. Figure 3 shows the lowest $\sigma(^{199}Hg)$ values for these two complexes. Besides, according to QTAIM, both W_2S_2, W_3S_6, the highest local energy minima, show that water molecules interact via O···O contacts instead of regular hydrogen bonds.

J(^{13}C−^{17}O) and J(^{199}Hg−^{13}C) couplings are related to hydrogen bonds. The complexes having

hydrogen bonds have a J(^{199}Hg$-^{13}$C) smaller than 4000Hz (Figure 4). As with the nuclear shielding, the J-couplings in W_3S_5 behave differently and present a singularity of unknown nature.

Even though the spatial configuration and the different interactions among water molecules do not significantly change the structure of CH_3Hg^+, the J-couplings and the σ nuclear shielding are widely influenced by the solvent. This suggests a new strategy to use J and σ in determining the local geometries in the microsolvation of methylmercury. For example, the combined values of J and σ could indicate the number of solvent molecules in the coordination sphere of CH_3Hg^+, as well as the type of interactions between solvent molecules.

Concluding remarks

In this work, we report a study of the microsolvation of methylmercury using scalar and full relativistic methods in the calculation of both, equilibrium structures and intrinsic and response properties. Inter and intramolecular interactions have been analyzed using the Quantum Theory of Atoms in Molecules (QTAIM). Nuclear magnetic shielding constants and indirect nuclear spin–spin couplings are also discussed.

At the SR level, 1, 2, 6 structures in the potential energy surface were located for 1, 2, 3 water molecules interacting with CH_3Hg^+ respectively. Our results suggest that SR HF geometries are acceptable, with minor to negligible changes when compared to the more expensive SR MP2 and to the extremely more expensive DHF calculations. The most stable complexes are energetically favored by a single Hg$\cdots$O interaction and to a lesser extent by larger number of hydrogen bonds. We provide evidence suggesting that methylmercury binds very strongly to just one water molecule via Hg$\cdots$O interactions and that additional water molecules solvate the $(CH_3Hg\cdots OH_2)^+$ complex. In addition, QTAIM results suggest that when a particular complex

presents two Hg$\cdots$O interactions, one of them is a highly formed bond with certain degree of covalency while the other is a weaker interaction of closed shell nature.

From a structural point of view, CH_3Hg^+ is not sensitive to solvent effects because methylmercury $\leftrightarrow$ water molecular interactions do not significantly change the geometry of methylmercury, this is clearly seen in the fact that calculated molecular structures of solvated CH_3Hg^+ match the geometries for isolated CH_3Hg^+, in addition, this result is nicely supported by excellent agreement with gas phase dimethylmercury electron diffraction experiments and by NMR studies of CH_3HgCl solvated in liquid crystals. Relativistic effects and electron correlation need both be included for accurate calculations of interaction energies. The $[CH_3Hg(H_2O)_{1,2,3}]^+$ complexes are thermodynamically stable with respect to dissociation into methylmercury and the corresponding number of isolated water molecules.

Considering the behavior of the two most important magnetic parameters of NMR we have analyzed, we found that they are quite sensitive to the solvation process of methylmercury. Relativistic effects are important or very important depending on the magnetic parameter analyzed. In the case of the Hg$\cdots$O interaction in W_1S_1, J(^{199}Hg$-^{17}$O) is highly relativistic. Its relativistic value is seven times larger than its NR counterpart. This means that the Hg – O coupling is mostly due to electronic effects. The analysis was carry out keeping the geometry of the structure fixed and scaling the velocity of light in calculations. Relativistic effects increase the value of $\sigma(^{199}\mathrm{Hg})$, while decrease $\sigma(^{13}\mathrm{C})$ and $\sigma(^{17}\mathrm{O})$. Even though such effects are fundamental for mercury (they contribute with up to 49% to σ), for carbon and oxygen they are not negligible (11% and 14% contributions to σ respectively). There is a highly correlated behavior among the shieldings of carbon and oxygen in each W_nS_m structure.

A crucial result is that NMR parameters, which are normally used to determine the molecular geometry, are greatly affected by the solvent. However, the structure of methylmercury remains

without significant changes due to the presence of water molecules. $\sigma(^{199}Hg)$ decreases as the number of Hg$\cdots$O contacts increase. A larger nuclear shielding in ^{199}Hg indicates larger energy stabilization. In addition, the number of hydrogen bonds has an inverse relationship with $\sigma(^{199}Hg)$. There is a strong correlation between $\sigma(^{13}C)$ and $\sigma(^{17}O)$. The solvent induces electronic effects along the C–Hg$\cdots$O interaction, suggesting that the Hg atom serves as an electronic link between the C and O atoms. $J(^{13}C-^{17}O)$ and $J(^{199}Hg-^{13}C)$ couplings are affected by hydrogen bonds.

From our results we can state that NMR spectroscopic parameters can be used as important experimental and theoretical tools to learn how many water molecules take part in the microsolvation process of Methlymercury.

Acknowledgements

Funding for this work was partially provided by Universidad de Antioquia via *"Estrategia para la sosenibilidad"* and by CODI internal project No. 10170. The authors thank APOLO, the Center for Scientific Computing at Universidad EAFIT and Juan David Pineda, the system administrator. The work in Argentina was supported by the Argentinian Agency for promotion of Science and Technology (FONCYT PICT2012-1214).

References

(1) M. F. Wolfe, S. Schwarzbach and R. A. Sulaiman. *"Environ. Toxicol. Chem.."* 17, no. 2 **(1998)**: 146-160.

(2) C. T. Driscoll, R. P. Mason, H. M. Chan, D. J. Jacob and N. Pirrone. *"Environ. Sci. Technol."* 47, no. 10, **(2013)**: 4967-4983

(3) F. Morel, M. L. Kraepiel and M. Amyot. *"Annu. Rev. Ecol. Syst."* 29 **(1998)**: 543-566.

(4) Z. Castilhos and E. D. Bidone. *"B. Environ. Contam Tox."* 64, no. 5, **(2000)**: 693-700.

(5) Z. C. Castilhos, E. D. Bidone and S. M. Hartz. *"B. Environ. Contam Tox."* 66. 5, **(2001)**: 631-637.

(6) G. Hincapie, N. Acelas, M. Castaño, J. David and A. Restrepo. *"J. Phys. Chem. A."* 114, no. 29 **(2010)**: 7809-7814.

(7) United Nations Environment Programme (UNEP). *"Minamata Convention Agreed by Nations. January 19, 2013."* http://www.unep.org/newscentre/Default.aspx?DocumentID=2702&ArticleID=9373&l=en (accessed May 12, 2014).

(8) United Nations Environment Programme (UNEP).*"Anexo: Proyecto del Convenio de Minamata sobre el Mercurio."* **(2013)**. http://www.unep.org/hazardoussubstances/Portals/9/Mercury/Documents/INC5/5_7_s_annex_advance.pdf (accessed May 12, 2014).

(9) P.A. Kumar. *"Microsolvation of Charged and Neutral Species: A Theoretical Study."* PhD Thesis. Bhabha National Institute: India. **(2009)**

(10) K. Räisänen, J. Kuonanoja and J. Jokisaari. *"Mol. Phys."* 38, no. 4 **(1979)**: 1307-1310.

(11) J. Jokisaari, K. Räisänen, J. Kuonanoja, P. Pyykkö and L. Lajunen. *"Mol. Phys."* 39, no. 3 **(1980)**: 715-723.

(12) J. Jokisaari, and P. Diehl. *"Org. Magn. Resonance"* 13, no. 5 **(1980)**: 359-362.

(13) J. Jokisaari, S. Järvinen, J. Autschbach and T. Ziegler. *"J. Phys. Chem. A"* 106, no. 40 **(2002)**: 9313-9318.

(14) J. Autschbach, A. M. Kantola and J. Jokisaari. *"J. Phys. Chem. A"* 111, no. 24 **(2007)**: 5343-5348.

(15) J. Autschbach and M. Sterzel. *"J. Am. Chem. Soc."* 129, no. 36 **(2007)**: 11093-11099.

(16) V. Arcisauskaite, J. I. Melo, L. Hemmingsen and S. Sauer. *"J. Chem. Phys."* 135, no. 4 **(2011)**: 044306.

(17) J. Roukala, A. F. Maldonado, J. Vaara, G. A. Aucar and P. Lantto. *"Phys. Chem. Chem. Phys."* 13, no. 47 **(2011)**: 21016-21025.

(18) D. L. Rabenstein, A. I. Anvarhusein and R. S. Reid. *"BBA-Mol Cell Res."* 720, no. 1 **(1982)**: 53-64.

(19) E. Buncel, C. Boone, H. Joly, R. Kumar and A. R. Norris. *"J. Inorg. Biochem."* 25, no. 1 **(1985)**: 61-73.

(20) D. L. Rabenstein, A. P. Arnold and R. D. Guy. *"J. Inorg. Biochem."* 28, no. 2 **(1986)**: 279-287.

(21) L. Girault, A. Boudou and E. J. Dufourc. *"BBA - Biomembranes."* 1325, no. 2 **(1997)**: 250-262.

(22) G. Schreckenbach and G. A. Shamov. *"Acc. Chem. Res."* 43, no. 1 **(2009)**: 19-29.

(23) Zheng, S.; Autschbach, J. *Chem. Eur. J*. **2011**, *17*, 161.

(24) Woff, S.; Ziegler, T.; van Lenthe, E.; Baerends, E. *J. Chem. Phys*. **1999**, *110*, 7689.

(25) Autschbach, J. *The calculation of NMR parameters in transition metal complexes*. Principles and Applications of Density Functional Theory in Inorganic Chemistry I. Springer Berlin Heidelberg, 2004. 1-48.

(26) Moncho, S.; Autschbach, J. *J. Chem. Theor. Comp*. **2010**, *6*, 223.

(27) J. I. Melo, M. Ruiz De Azúa, C. G. Giribet, G. A. Aucar and R. H. Romero. *"J. Chem. Phys."* 118, no. 2 **(2003)**: 471-486.

(28) J. I. Melo, M. Ruiz De Azúa, C. G. Giribet, G. A. Aucar and P. F. Provasi. *"J. Chem. Phys."* 121, no. 14 **(2004)**: 6798-6808.

(29) G. A. Aucar and J. Oddershede. *"Int. J. Quantum Chem."* 47, no. 6 **(1993)**: 425-435

(30) G. A. Aucar, R. H. Romero and A. F. Maldonado. *"Int. Rev. on Phys. Chem."* 29, no. 1 **(2010)**: 1-64

(31) G. A. Aucar. *"Phys. Chem. Chem. Phys."* 16, no. 10 **(2014)**: 4420-4438

(32) R. H. Romero and G. A. Aucar *"Phys. Rev. A."* 65, no. 5 **(2002)**: 053411

(33) R. H. Romero and G. A. Aucar *"Int. J. Molec. Sci."* 3, no. 8 **(2002)**: 914-930

(34) DIRAC, a relativistic ab initio electronic structure program, Release DIRAC13 (2013), written by L. Visscher, H. J. Aa. Jensen, R. Bast, and T. Saue, with contributions from V. Bakken, K. G. Dyall, S. Dubillard, U. Ekström, E. Eliav, T. Enevoldsen, E. Faßhauer, T. Fleig, O. Fossgaard, A. S. P. Gomes, T. Helgaker, J. K. Lærdahl, Y. S. Lee, J. Henriksson, M. Iliaš, Ch. R. Jacob, S. Knecht, S. Komorovský, O. Kullie, C. V. Larsen, H. S. Nataraj, P. Norman, G. Olejniczak, J. Olsen, Y. C. Park, J. K. Pedersen, M. Pernpointner, K. Ruud, P. Sałek, B. Schimmelpfennig, J. Sikkema, A. J. Thorvaldsen, J. Thyssen, J. van Stralen, S. Villaume, O. Visser, T. Winther, and S. Yamamoto (see http://www.diracprogram.org).

(35) G. A. Aucar, T. Saue, L. Visscher and H. J. Aa. Jensen *"J. Chem. Phys."* 110, no. 13 **(1999)**: 6208-6218

(36) J. Pérez y A. Restrepo. *"ASCEC V-02: Annealing Simulado con Energía Cuántica."* Property, development and implementation: Grupo de Química-Física Teórica, Instituto de Química, Universidad de Antioquia: Medellín, Colombia. **(2008)**

(37) N. Metropolis, A. Rosenbluth, M. Rosenbluth, A. Teller, and E. Teller. *"J. Chem. Phys."* 21, no. 6 **(1953)**: 1087-1092.

(38) S. Kirkpatrick, D. Gelatt, and M. Vecchi. *"Science."* 220, no. 4598 (1983): 671-680.

(39) P. Van Laarhoven and E. Aarts. *"Simulated annealing: theory and applications."* Vol. 37. Springer Science & Business Media, 1987.

(40) J. Pérez, E. Florez, C. Hadad, P. Fuentealba and A. Restrepo. *"J. Phys. Chem. A"* 112, no. 25 **(2008)**: 5749-5755.

(41) J. Pérez, C. Hadad and A. Restrepo. *"Int. J. Quantum Chem."* 108, no. 10 **(2008)**: 1653-1659.

(42) J. David, D. Guerra and A. Restrepo. *"J. Phys. Chem. A."* 113 **(2009)**: 10167.

(43) J. Murillo, J. David and A. Restrepo. *"Phys. Chem. Chem. Phys."* 12 **(2010)**: 10963.

(44) J. David, D. Guerra, C. Hadad and A. Restrepo. *"J. Phys. Chem. A."* 114 **(2010)**: 10726.

(45) F. Ramírez, C. Hadad, D. Guerra, J. David and A. Restrepo. *"Chem. Phys. Lett."* 507 **(2011)**: 229.

(46) J. Romero, A. Reyes, J. David and A. Restrepo. *"Phys. Chem. Chem. Phys."* 13 **(2011)**: 15264.

(47) J. David, D. Guerra and A. Restrepo. *"Chem. Phys. Lett."* 64 **(2012)**: 539âĂŞ540.

(48) D. Yepes, S. Kirk, S. Jenkins and A. Restrepo. *"J. Mol. Model."* 18 **(2012)**: 4171.

(49) C. Ibargüen, M. Manrique-Moreno, C. Hadad, J. David and A. Restrepo. *"Phys. Chem. Chem. Phys."* 15 **(2013)**: 3203

(50) J. D. Gonzalez, E. Flórez, J. Romero, A. Reyes and A. Restrepo. *"J. Mol. Model."* 19 **(2013)**: 1763.

(51) S. Gomez, D. Guerra, J. David and A. Restrepo. *"J. Mol. Model."* 19 **(2013)**: 2173.

(52) C. Hadad, A. Restrepo, S. Jenkins, F. Ramírez and J. David. *"Theor. Chem. Acc."* 132 **(2013)**: 1376.

(53) N. Acelas, G. Hincapié, D. Guerra, J. David and A. Restrepo. *"J. Chem. Phys."* 139 **(2013)**: 044310.

(54) D. Guerra, J. David and A. Restrepo. *"J. Comput. Meth. Sci. Eng."* 14 **(2014)**: 93âĂŞ102.

(55) A. Zapata-Escobar, M. Manrique-Moreno, D. Guerra, C. Hadad and A. Restrepo. *"J. Chem. Phys."* 140 **(2014)**: 184312.

(56) C. Hadad, E. Florez, G. Merino, J. L. Cabellos, F. Ferraro and A. Restrepo. *"J. Phys. Chem. A."* 118 **(2014)**: 5762.

(57) A. Echeverri, N. Moreno, A. Restrepo and C. Hadad. *"Chem. Phys. Lett."* 16 **(2014)**: 615.

(58) C. Ibargüen, D. Guerra, C. Hadad and A. Restrepo. *"RSC Adv."* 4 **(2014)**: 58217.

(59) Gaussian 09, Revision D.01, M. J. Frisch, G. W. Trucks, H. B. Schlegel, G. E. Scuseria, M. A. Robb, J. R. Cheeseman, G. Scalmani, V. Barone, B. Mennucci, G. A. Petersson, H. Nakatsuji, M. Caricato, X. Li, H. P. Hratchian, A. F. Izmaylov, J. Bloino, G. Zheng, J. L. Sonnenberg, M. Hada, M. Ehara, K. Toyota, R. Fukuda, J. Hasegawa, M. Ishida, T. Nakajima, Y. Honda, O. Kitao, H. Nakai, T. Vreven, J. A. Montgomery, Jr., J. E. Peralta, F. Ogliaro, M. Bearpark, J. J. Heyd, E. Brothers, K. N. Kudin, V. N. Staroverov, T. Keith, R. Kobayashi, J. Normand, K. Raghavachari, A. Rendell, J. C. Burant, S. S. Iyengar, J. Tomasi, M. Cossi, N. Rega, J. M. Millam, M. Klene, J. E. Knox, J. B. Cross, V. Bakken, C. Adamo, J. Jaramillo, R. Gomperts, R. E. Stratmann, O. Yazyev, A. J. Austin, R. Cammi, C. Pomelli, J. W. Ochterski, R. L. Martin, K. Morokuma, V. G. Zakrzewski, G. A. Voth, P. Salvador, J. J. Dannenberg, S. Dapprich, A. D. Daniels, O. Farkas, J. B. Foresman, J. V. Ortiz, J. Cioslowski, and D. J. Fox, Gaussian, Inc., Wallingford CT, **(2013)**.

(60) F. Weigend, M. Häser, H. Patzelt and R. Ahlrichs. *"Chem. Phys. Lett."* 294, no. 1 **(1998)**: 143-152.

(61) Dyall, K. *Chem. Phys. Lett*. **1994**, *224*, 186–194.

(62) Laerdahl, J.; Saue, T.; Faegri , K. *Theor. Chem. Acc*. **1997**, *97*, 177–184.

(63) van Stralen, J.; Visscher, L.; Larsen, C.; Jensen, H. *Chem. Phys*. **2005**, *311*, 81–95.

(64) K. Kashiwabara, S. Konaka, T. Iijima and M. Kimura. *"Bull. chem. Soc. Japan."* 46, **(1973)**: 407.

(65) Gutowski, M.; Skurski, P.; Boldyrev, A.; Simons, J.; Jordan, K. *Phys. Rev. A*, **1996**, *54*(3), 1906.

(66) Peterson, K.; Dunning, T. *J. Chem. Phys*. **1995**, *102*(5), 2032–2041.

(67) Rosen, A.; Ellis, D. *J. Chem. Phys*. **1975**, *62(8), 3039–3049.*

(68) Giménez, C.; Maldonado, A.; Aucar, G. In preparation.

(69) Maldonado, A.; Aucar, G. J. Phys. Chem. A. **2014***,* 118*, 7863–7875.*

(70) Malli, Gulzari, ed. Relativistic and electron correlation effects in molecules and solids. Vol. 318. Springer Science & Business Media, 2013.

(71) R. Bader, "Atoms in Molecules: A Quantum Theory." *Clarendon Press, Oxford **(1994)***

(72) T. Keith, "AIMALL version 13.05.06,." *TK Gristmill Software **(2013)**. Overland Park KS, USA (see aim.tkgristmill.com)*

(73) E. A. Zhurova, V. G. Tsirelson, A. I. Stash and A. A. Pinkerton. "J. Am. Chem. Soc." *124, no. 17 **(2002)**: 4574-4575.*

(74) A. H. Pakiari and K. Eskandari "J. Mol. Struct. THEOCHEM." *806, no. 1 **(2007)**: 1-7.*

(75) S. Jenkins, A. Restrepo, J. David, D. Yin and S. R. Kirk. "Phys. Chem. Chem." *Phys 13, no. 24 (2011): 11644-11656.*

(76) P.L.A. Popelier. "Atoms in Molecules: an Introduction." *Prentice Hall, Pearson Education Limited, **(2000)**.*

(77) D. Cremer and E. Kraka, "Angew. Chem. Int. Ed. Engl." *23 **(1984)**: 627-628.*

(78) Grabowski, S. Chem. Rev. **2011**, 111 *2597.*

(79) *Rozas, I.; Alkorta, I.; Elguero, J.* J. Am. Chem. Soc. **2000**, 122 *11154.*

(80) *X. Fradera, M. A. Austen and R. Bader.* "J. Chem. Phys. A." *103, no. 2* ***(1999)****: 304-314.*

(81) *E. Espinosa, I. Alkorta, J. Elguero and E. Molins.* "J. Chem. Phys." *117, no. 12* ***(2002)****: 5529-5542.*

(82) *Rojas–Valencia, N.; Ibargüen, C.; Restrepo, A.* Chem. Phys. Lett. **2015**, 635, *301.*

(83) *Hernández–Cobos, J.; Ramírez–Solís, A.; Maron, L.; Ortega–Blake, I.* J. Chem. Phys. **2012**, 136, *014502.*

(84) *Persson, I.; Sandström, M.; Goggin, P.; Mosset, A.* J. Chem. Soc. Dalton Trans. **1985**, 8, *1597.*

(85) *Sandström, M.; Persson, I.; Goggin, P.* J. Chem. Soc. Dalton Trans. **1987**, 10, *2411.*

(86) *Abraham, M.; Gil–Lostes, J.; Acree, W.; Cometto–Muñiz, E.; Cain, W.* J. Environ. Monit. **2008**, 10, *435.*

(87) *Persson, I.; Landgren, M.; Marton, A.* Inorg. Chim. Acta. **1986**, 116, *135.*

(88) *Soldán, P.; Lee, E.; Wright, T.* J. Phys. Chem. A. **2002**, 106, *8619.*

(89) *Tossell, J.* J. Phys. Chem. A. **2001**, 105, *935.*

(90) *Shepler, B.; Wright, A.; Balabanov, N.; Peterson, K.* J. Phys. Chem. A. **2007**, 111, *11342.*

(91) *Amaro–Estrada, J.; Ramírez–Solís, A.* Comp. Theor. Chem. **2013**, 1006, *47.*

(92) *P. Pyykkö, A. Görling and N. Rösch.* "Mol. Phys." *61, no. 1* ***(1987)****: 195-205.*

(93) *M. Kaupp, O. L. Malkina, V. G. Malkin, and P. Pyykkö.* Chem. A Eur. J. *4, no. 1* ***(1998)****: 118-126.*

(94) *U. Edlund, T. Lejon, P. Pyykkö, T. K. Venkatachalam and E. Buncel.* J. Am. Chem. Soc. *109, no. 20* ***(1987)****: 5982-5985.*

(95) *P. Lantto, R. H. Romero, S. S. Gómez, G. A. Aucar and J. Vaara.* J. Chem. Phys. *125, no. 18* ***(2006)****: 184113.*

(96) *A. F. Maldonado and G. A. Aucar.* "Phys. Chem. Chem. Phys. *11, no. 27* ***(2009)****: 5615-5627.*

(97) *Maldonado, A.; Melo, J.; Aucar, G.* Phys. Chem. Chem. Phys. **2015**, 17, *25516–25524.*

(98) *A. F. Maldonado, G. A. Aucar and J. I. Melo.* J. Mol. Model. *20, no. 9* ***(2014)****: 2417.*